The $CH_3 + HO_2$ Reaction: First-Principles Prediction of Its Rate Constant and Product Branching Probabilities

Rongshun Zhu and M. C. Lin*

Department of Chemistry, Emory University, Atlanta, Georgia 30322

Received: February 22, 2001; In Final Form: April 23, 2001

The reaction of the CH_3 radical with HO_2 has been investigated by means of ab initio molecular orbital theory and variational RRKM theory calculations. The reaction can take place by several product channels producing (a) $CH_4 + O_2$ ($^3\Sigma_g^-$) and (b) $CH_4 + O_2$ ($^1\Delta$) by direct H abstraction and (c) $CH_3O + OH$ and (d) $CH_2O + H_2O$ by an association/decomposition mechanism via CH_3OOH. The bimolecular reaction rate constants for the formation of these products have been calculated for the temperature range 300−3000 K and found to be pressure independent up to 50 atm. The Arrhenius equations for the two major channels a and c were found to be strongly curved; they can be represented by $k_a = 4.23 \times 10^{-16}T^{1.25}\exp(828/T)$ for 300−800 K, $k_a = 3.02 \times 10^{-21}T^{2.83}\exp(1877/T)$ for 800−3000 K, and $k_c = 2.97 \times 10^{-10}T^{-0.24}\exp(182/T)$ for 300−1000 K and $1.02 \times 10^{-13}T^{0.76}\exp(1195/T)$ for 1000−3000 K, in units of cm^3 $molecule^{-1}$ s^{-1}. In the abstraction channel a, the effect of multiple reflections above its van der Waals complex ($CH_3\cdots HO_2$), which lies 1.9 kcal/mol below the reactants with a 1.2 kcal/mol barrier leading to the formation of the $CH_4 + O_2$ ($^3\Sigma_g^-$) products, was found to be quite significant at low temperatures ($T < 300$ K). In addition, the predicted rate constant for the unimolecular decomposition of CH_3OOH agrees closely with the available experimental data using the heats of formation of CH_3O (5.4 ± 0.5 kcal/mol) and CH_3OOH (−29.0 ± 1.0 kcal/mol) calculated with the isodesmic method at 0 K.

1. Introduction

The reaction of CH_3 with HO_2 plays a pivotal role in the combustion of small hydrocarbons,[1−7] particularly under moderate temperature (<1700 K) and high-pressure (>40 atm) conditions.[5] The reaction has been shown to be highly influential on the evaluation of the $CH_3 + O_2$ reaction rate constant, because of the strong kinetic coupling in the complex chemistry of the $CH_4 + O_2$ oxidation reaction.[7]

The kinetics for the $CH_3 + HO_2$ reaction has not yet been reliably determined experimentally because, in part, of the high degree of difficulty in measuring the concentrations of both radical reactants accurately for rate constant determination. The reaction is highly exothermic and it can conceivably take place via several product channels by the direct and indirect bimolecular reaction mechanisms as shown below:

The direct abstraction channels:

$$CH_3 + HO_2 \rightarrow CH_4 + O_2\ (^3\Sigma_g^-) \quad \text{(a)}$$

$$\rightarrow CH_4 + O_2\ (^1\Delta) \quad \text{(b)}$$

The association/decomposition channels:

$$CH_3 + HO_2 \rightleftharpoons CH_3OOH^\dagger \rightarrow CH_3O + OH \quad \text{(c)}$$

$$\rightarrow CH_2O + H_2O \quad \text{(d)}$$

$$\rightarrow CH_3OOH\ (+M) \quad \text{(e)}$$

where the † represents internal excitation. Among these elementary reaction steps; only the thermal decomposition of methylhydroperoxide (CH_3OOH) associated with step c has been studied experimentally.[8,9] The exothermicities for the formation of these products can be found in Table 1 (vide infra). For a reliable prediction of the total rate constant and product branching probabilities under chemically activated conditions, a full characterization of the potential energy surfaces (PESs) involving both mechanisms is essential.

In this study, we calculate the PES of the whole system with the G2M method[10] and estimate the rate constants for individual product channels employing transition-state theory (TST) for the direct abstraction process and the variational Rice−Ramsperger−Kassel−Marcus (RRKM) theory[11] for the indirect bimolecular reaction via $CH_3OOH^\dagger$. These computational methods will be presented in detail below.

2. Computational Methods

Ab Initio Calculations. The geometry of the reactants, intermediates, transition states, and products of the $CH_3 + HO_2$ reaction were optimized at the B3LYP/6-311G(d,p) level with Becke's three-parameter nonlocal exchange functional[12−14] with nonlocal correlation functional of Lee et al.[15] The energies of all species were calculated by the G2M method,[10] which uses a series of calculations with B3LYP/6-311G(d,p) optimized geometries to approximate the CCSD(T)/6-311+G(3df,2p) level of theory, including a "higher level correction" (HLC) based on the number of paired and unpaired electrons. The total G2M energy with zero-point energy (ZPE) correction is calculated as follows:

$$E[\text{G2M(RCC, MP2)}] = E[\text{RCCSD(T)/6-311G(d,p)}] + \Delta E(+3\text{df, 2p}) + \Delta E(\text{HLC}) + \text{ZPE[B3LYP/6-311G(d,p)]}$$

* To whom correspondence should be addressed. E-mail: chemmcl@emory.edu.

10.1021/jp010698i CCC: $20.00
Published on Web 05/31/2001

TABLE 1: Total and Relative Energies of Reactants, Intermediates, Transition States, and Products for the Reaction of CH_3 with HO_2 Calculated at Different Levels of Theory with B3LYP/6-311G(d,p) Optimized Geometries

		energies[a]			
species	ZPE[b]	MP2/ 6-311G(d,p)	MP2/ 6-311+G(3df,2p)	CCSD(T)/ 6-311G(d,p)	G2M
$CH_3 + HO_2$	27.4	−190.292 462 8	−190.407 916 8	−190.346 728	−190.468 25
$CH_2O + H_2O$	30.0	−129.5	−135.9	−119.1	−126.1
$CH_3O + OH$	28.0	−22.4	−28.8	−16.6	−24.1
$CH_4 + {}^3O_2$	30.3	−69.2	−66.3	−60.7	−58.2
$CH_4 + {}^1O_2$	30.3	−37.2	−36.2	−30.1	−29.4
vdW	28.9	−4.2	−3.9	−3.7	−1.9
CH_3OOH	34.1	−76.2	−81.2	−69.0	−70.5
TS1	29.5	−22.4	−28.8	−16.6	−24.1
TS2	27.8	0.8	0.9	−1.1	−0.7
TS3	30.1	11.4	8.3	7.8	4.1

[a] The total energies of $CH_3 + HO_2$ are in units of a.u., and the relative energies are in units of kcal/mol; the ZPE are included only in G2M energies. [b] The zero-point energies are calculated at the B3LYP/6-311G** level, and the values are in units of kcal/mol.

$$\Delta E(+3\mathrm{df},\,2\mathrm{p}) = E[\mathrm{MP2/6\text{-}311 + G(3df,\,2p)}] - E[\mathrm{MP2/6\text{-}311G(d,p)}]$$

$$\Delta E(\mathrm{HLC}) = -0.005\ 25n_\beta - 0.000\ 19n_\alpha$$

where n_α and n_β are the numbers of valence electrons, $n_\alpha \geq n_\beta$. All calculations were carried out with Gaussian 98[16] and MOLPRO 96[17] programs.

Rate Constant Calculations. The rate constants were computed with a microcanonical variational RRKM methods[18−20] which solves the master equation[18−23] involving multistep vibrational energy transfers for the excited intermediate ($CH_3O_2H^\dagger$). The PES calculated at the G2M level, to be discussed in the next section, was used in the calculation.

Similar to our previous calculations[24−27] with the Variflex code,[18] the component rates were evaluated at the E,J-resolved level. The effect of pressure was studied by 1-D master equation calculations using the Boltzmann probability of the complex for the J distribution. The master equation was solved by an inversion based approach.[18−20] To achieve convergence in the integration over the energy range, an energy grain size of 100 cm^{-1} was used; this grain size provides numerically converged results for all temperatures studies with the energy spanning range from 15 000 cm^{-1} below to 64 900 cm^{-1} above the threshold. The total angular momentum J covered the range from 1 to 241 in steps of 10 for the E,J-resolved calculation. For the barrierless transition states, the Varshni potential[28]

$$V(R) = D_e\{1 - \alpha \exp[-\beta(R^2 - R_0^2)]\}^2 - D_e$$

was used to represent the potential energy along the individual reaction coordinate. In the above equation, D_e is the bond energy of CH_3-O_2H or CH_3O-OH, excluding zero-point vibrational energies; $\alpha = R_0/R$, where R is the reaction coordinate (i.e., the distance between the two bonding atoms, in the present case C−O, or O−O), and R_0 is the equilibrium value of R. For the tight transition states, the numbers of states were evaluated according to the rigid-rotor harmonic-oscillator approximation.

3. Results and Discussion

A. Potential-Energy Surface and Reaction Mechanism. The optimized geometries of the reactants, intermediates, transition states, and products are shown in Figure 1; the potential energy diagram obtained at the G2M level is presented in Figure 2; the total and relative energies are compiled in Table 1; and the vibrational frequencies and moments of inertia of all species used in RRKM calculations are summarized in Table 2. As illustrated in Figure 2, the $CH_3 + HO_2$ reaction can occur via several product channels as alluded to before.

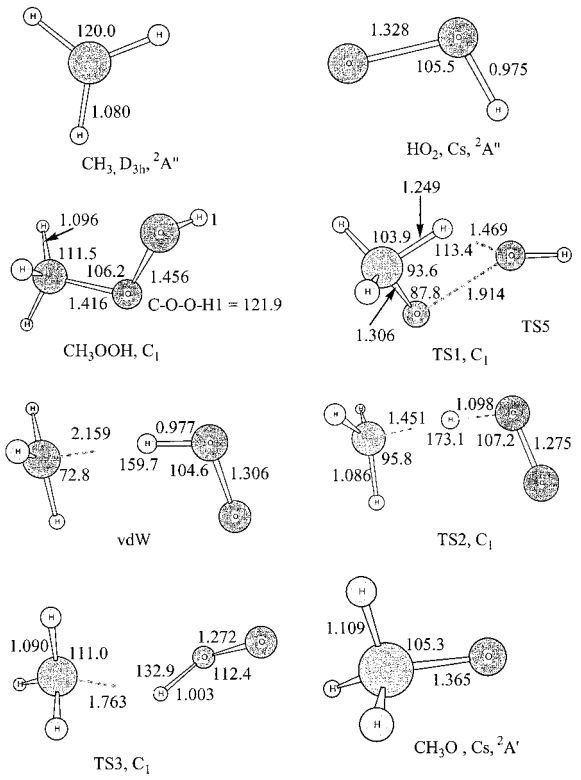

Figure 1. Optimized geometries of the reactants, intermediates, transition states, and products (except O_2, H_2O, OH, CH_2O, and CH_4) computed at the B3LYP/6-311G(d,p) level.

H-Atom Abstraction Reaction. As shown in Figure 2, the H-abstraction reaction can take place through a triplet PES via a van der Waals complex, vdW, with C_1 symmetry. The complex is more stable than the $CH_3 + HO_2$ reactants by 1.9 kcal/mol at the G2M level; it fragments readily via TS2 with a small (1.2 kcal/mol) barrier to give CH_4 and the ground-state molecule O_2 ($^3\Sigma_g^-$) with an overall exothermicity of 58.2 kcal/mol. From Figure 1, one can see that the C−H−O bond angle in TS2 is about 14° larger than that in vdW and the newly forming C−H bond length decreases from 2.159 Å in vdW to 1.45 Å in TS2. For both vdW and TS2, the HO_2 and the C atom of the CH_3 radical are in the same plane. The CH_3 can also directly abstract the H atom from HO_2 through a singlet surface via TS3 to produce CH_4 and the excited O_2 ($^1\Delta$) molecule. The barrier and exothermicity of this channel are 4.1

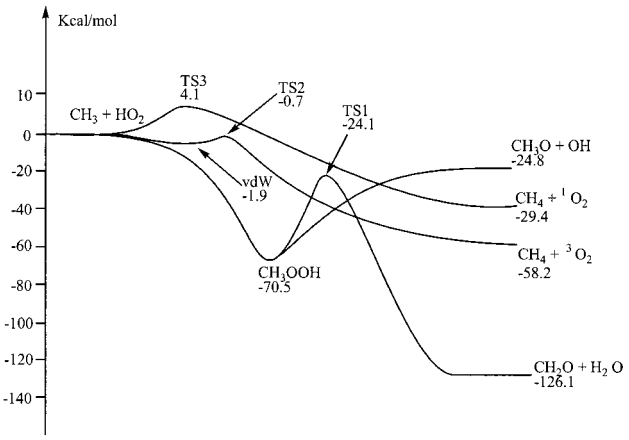

Figure 2. Schematic energy diagram of the CH_3-HO_2 system computed at the G2M level.

and 29.4 kcal/mol, respectively. It is worth noting that an extensive search for an analogous path producing the excited O_2 from CH_3OOH unimolecularly failed to locate its transition state.

Association/Decomposition Channels. The association reaction of CH_3 and HO_2 by a barrierless process forms methylhydroperoxide, CH_3OOH, which has C_1 symmetry with 121.9° dihedral angle C−O−O−H_1. CH_3OOH lies 70.5 kcal/mol below the reactants at the G2M level. A further discussion on the heat of the formation of the peroxide molecule will be made later in conjunction with its thermal unimolecular decomposition reaction. The internally excited $CH_3OOH^{\dagger}$ can dissociate via TS1 producing $CH_2O + H_2O$ by a concerted H-migration/H_2O-elimination mechanism. No experimental data are available for this channel, although it is the most exothermic process with the exothermicity of 126.1 kcal/mol. To our knowledge, this calculation represents the first ab initio study on the reaction channel. TS1 lies 24.1 kcal/mol below the reactants and 46.4 kcal/mol above the intermediate with C_1 symmetry. The breaking O−O bond in TS1 is 0.498 Å longer than that in CH_3OOH, and the newly forming O−H bond in TS1 is 1.469 Å. As depicted in Figure 2, CH_3OOH can also decompose directly by breaking the O−O bond to give $CH_3O + OH$. This dissociation process occurs barrierlessly without a well-defined TS with an endothermicity of 45.7 kcal/mol above CH_3OOH at the G2M level of theory.

B. Rate Constant Calculations. Variational TST and RRKM calculations have been carried out for this reaction with the Variflex code[18−20] including the following reaction channels:

$$CH_3 + HO_2 \rightarrow CH_4 + O_2\ (^3\Sigma_g^-) \quad \text{(a)}$$

$$\rightarrow CH_4 + O_2\ (^1\Delta) \quad \text{(b)}$$

$$CH_3 + HO_2 \rightleftharpoons CH_3OOH^{\dagger} \rightarrow CH_3O + OH \quad \text{(c)}$$

$$\rightarrow CH_2O + H_2O \quad \text{(d)}$$

$$\rightarrow CH_3OOH\ (+M) \quad \text{(e)}$$

The energies used in the calculation are plotted in Figure 2, and the vibrational frequencies and moments of inertia are listed in Table 2. The LJ parameters required for the RRKM calculation of the unimolecular decomposition of CH_3OOH are approximated to be the same as those of CH_3OH ($\epsilon = 385.2$ K and $\sigma = 3.657$ Å).[29]

H-Abstraction Reactions. As mentioned in the previous section, the H atom of HO_2 can be abstracted by the CH_3 radical via the triplet or singlet surface to produce CH_4 and O_2 ($^3\Sigma_g^-$) or O_2 ($^1\Delta$), respectively. The formation of O_2 ($^3\Sigma_g^-$) by channel a takes place by the vdW. Our calculated results show that, at high temperatures, the rate constant is mainly controlled by the transition state (TS2) connecting the vdW and the $CH_4 + O_2$ ($^3\Sigma_g^-$) products. We have examined the effect of multiple reflections above the well of the vdW complex using the method of Hirschfelder and Wigner[30] as discussed by Miller.[31] The effect was found to be <1% at high temperatures (>2000 K); however, it becomes much stronger at low temperatures (T < 300 K) as illustrated in Figure 3. The predicted rate constant shown in Figure 3 reveals a weak negative temperature dependence below 800 K and a small positive temperature dependence above 800 K. The predicted result agrees reasonably with the value estimated by Tsang and Hampson[32] (see Figure 3).

The formation of O_2 ($^1\Delta$) by channel b proceeds directly via TS3 with 4.1 kcal/mol barrier. The rate constant (k_b) has a positive temperature dependence between 300 and 3000 K and is much smaller than k_a because of the higher barrier. It should be pointed out that the lowest vibrational modes, 17 cm^{-1} in TS2 and 59 cm^{-1} in TS3, were treated as classical one-dimensional free rotors in our rate constant calculations. The predicted two rate constants in the 300−3000K range can be represented by the expressions in units of cm^3 $molecule^{-1}$ s^{-1}:

$$k_a = 4.23 \times 10^{-16} T^{1.25} \exp(828/T), \quad 300-800\ \text{K}$$

$$k_a = 3.02 \times 10^{-21} T^{2.83} \exp(1877/T), \quad 800-3000\ \text{K}$$

$$k_b = 2.28 \times 10^{-19} T^{2.18} \exp(-1181/T), \quad 300-3000\ \text{K}$$

Bimolecular Association/Decomposition Reactions. As aforementioned, the association reaction of CH_3 with HO_2 producing methyl hydroperoxide occurs without a well-defined transition state because of the absence of a reaction barrier. To reliably predict the association rate, the flexible variational transition state approach originally developed by Marcus and co-workers[33,34] has been employed by means of the Variflex code as alluded to above. The association potential energy for the approach of CH_3 to HO_2 forming CH_3OOH was calculated by varying the forming C−O bond distance from 3.4 Å to its equilibrium value, 1.4163 Å, with an interval of 0.1 Å. Other geometric parameters were fully optimized with the C−O−O−H_1 dihedral angle fixed at 121.9° for each C−O separation at the B3LYP/6-311G(d,p) level of theory. For each structure, we calculated the 3N-7 vibrational frequencies, projected out of the gradient direction. The B3LYP-calculated total energies at each point were fitted by a Varshni potential energy function[28] given previously and then scaled to match the dissociation energy predicted at the G2M level of theory. The value of β in the Varshni potential was determined to be 0.628 $Å^{-2}$. A similar calculation has been performed for the decomposition of CH_3OOH to $CH_3O + OH$ which also occurs without a well-defined transition state. The dissociation potential energy function was obtained by varying the breaking O−O bond from the equilibrium value, 1.456 Å, to 3.2 Å at an interval of 0.1 Å. The computed potential energies could be fitted by the Varshni function with the parameters $\beta = 1.005$ $Å^{-2}$ and $D_e = 49.3$ kcal/mol (without ZPE correction). The dissociation energy was based on the heat of formation of CH_3OOH, -29.0 ± 1.0 kcal/mol, evaluated by the four isodesmic calculations listed in Table 3. This value compares reasonably with those estimated by

TABLE 2: Vibrational Frequencies and Moments of Inertia Used in Rate Constant Calculations for the Main Species of the $CH_3 + HO_2$ Reaction at the B3LYP/6-311G(d,p) Level of Theory

species	I_i (au)	frequencies
CH_3	6.3, 6.3, 12.6	504, 1403, 1403, 3105, 3284, 3284
HO_2	2.9, 53.6, 56.5	1162, 1427, 3610
CH_2O	6.3, 46.2, 52.6	1202, 1270, 1539, 1827, 2868, 2917
CH_3O	11.4, 64.6, 65.0	710, 963, 1108, 1360, 1371, 1518, 2890, 2955, 2995
OH	3.2, 3.2	3704
CH_3OOH	41.6,173.3,198.9	143, 252, 446, 876, 1037, 1171, 1205, 1372, 1451, 1457, 1512 3002, 3067, 3107, 3777
vdW	57.6, 380.2,1425.3	96, 106, 142, 147, 289, 415, 649, 1271, 1448, 1454, 1495, 3155, 3345, 3353, 3579
TS1	54.9, 183.8, 226.1	1544 ***i***, 204, 472, 509,631, 1069, 1091, 1230, 1244, 1287, 1516, 1789, 2946, 3037, 3610
TS2	38.6, 349.6, 374.5	542 ***i***, 17, 170.0, 268, 373, 476, 1008, 1428, 1446, 1484, 1854, 3056, 3078, 3194, 3221
TS3	47.9, 304.7, 340.4	2111 ***i***, 59, 150.0, 382, 509, 618, 1006, 1134, 1447, 1451, 1452, 1530, 3128, 3299, 3305

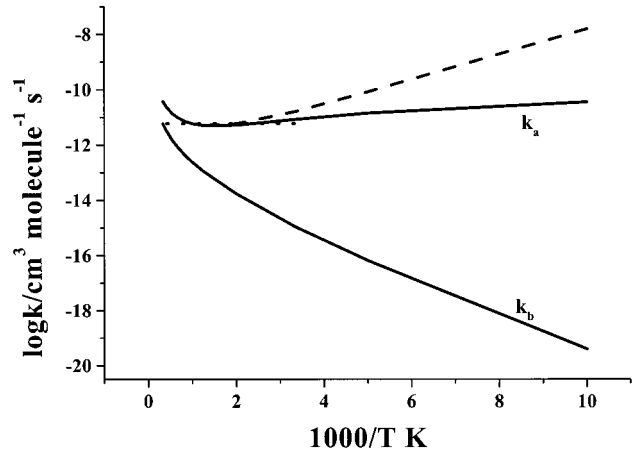

Figure 3. Predicted abstraction rate constants for $CH_3 + HO_2 \rightarrow CH_4 + O_2$ ($^3\Sigma_g$) and $CH_3 + HO_2 \rightarrow CH_4 + O_2$ ($^1\Delta$). The solid line is the predicted results with multiple reflections; the dashed line is the predicted results without including multiple reflections; and the dotted line is the estimated value from ref 32.

TABLE 3: Heat Formation of CH_3OOH Calculated by the Isodemic Method at the G2M Level[a]

reaction	$\Delta_r H^0$ (0K)	$\Delta_f H^0$ (CH_3OOH, 0K)
$CH_3OH + NO_2 \rightarrow CH_3OOH + NO$	29.8	-28.5 ± 0.3
$CH_3O + HOOH \rightarrow CH_3OOH + OH$	4.8	-30.0 ± 0.21
$CH_3 + HOOH \rightarrow CH_3OOH + H$	17.1	-29.9 ± 0.18
$CH_3OH + HOOH \rightarrow CH_3OOH + H_2O$	-8.8	-28.0 ± 0.13
average		-29.0 ± 1.0

[a] Values are in units of kcal/mol. The heats of formation reference species at 0 K were taken from ref 39, except that of CH_3O from ref 26. The errors given in the calculated values convolute all reported experimental ones.

Benson, -27.6 ± 1.0 kcal/mol (0 K),[35] and Lightfoot et al., -30.5 kcal/mol (0 K).[9]

The individual bimolecular reaction rate constants calculated under the atmospheric condition are displayed in Figure 4. The result clearly shows that the channel forming CH_3O and OH dominates, and the association process producing CH_3OOH has a strong negative temperature effect with only a small contribution to the total bimolecular rate constant under the atmospheric pressure condition. The rate constants for the bimolecular reactions of $CH_3 + HO_2 \rightarrow CH_3O + OH$ and $CH_3 + HO_2 \rightarrow H_2O + CH_2O$ were found to be pressure independent up to 50 atm. The rate constants can be expressed in units of cm^3 $molecule^{-1}$ s^{-1} by $k_c = 2.97 \times 10^{-10} T^{-0.24} \exp(182/T)$ for 300−1000 K, $k_c = 1.02 \times 10^{-13} T^{0.76} \exp(1195/T)$ for 1000−3000 K, and $k_d = 1.84 \times 10^{-19} T^{1.86} \exp(1238/T)$ covering the temperature range of 300−3000 K. Our theoretically predicted total rate constant is slightly higher than those estimated by Baulch et al.[36] and Tsang and Hampson.[32]

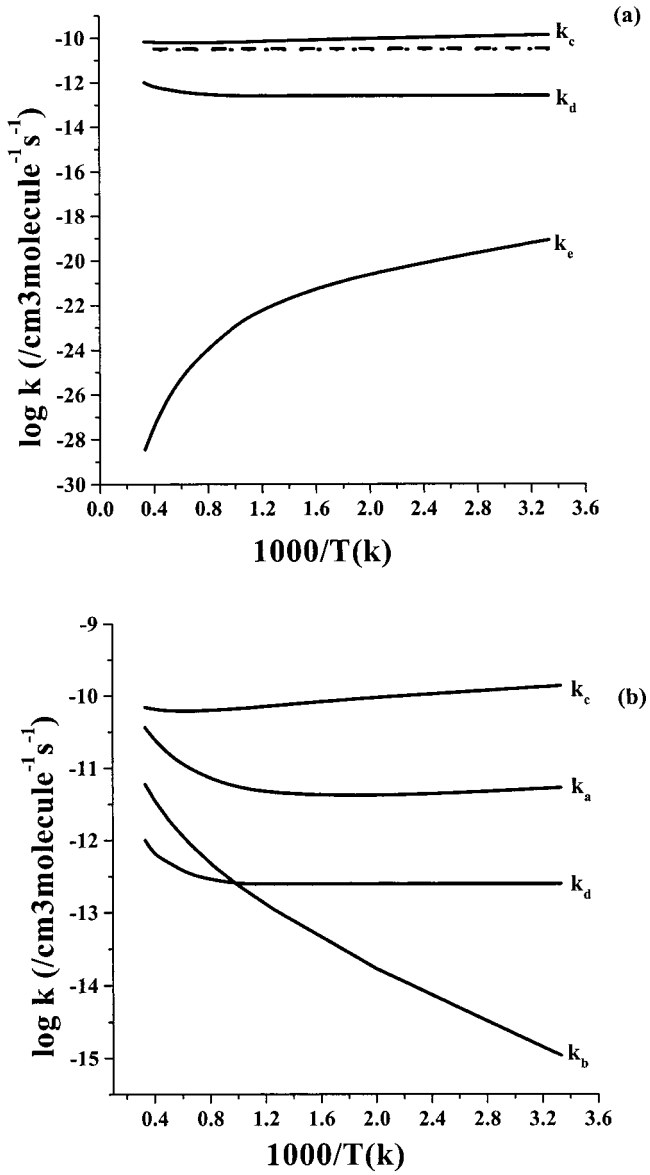

Figure 4. (a) Theoretically predicted bimolecular rate constants of k_c, k_d, and k_e. Dotted and dashed lines are the recommended values by refs 32 and 36, respectively; (b) Comparison of k_a, k_b, k_c, and k_d.

Unimolecular Decomposition of CH_3OOH. The unimolecular decomposition of CH_3OOH is the only process which has been experimentally measured.[8,9,36,37] The theoretically predicted dissociation rate constants for the decomposition reaction $CH_3OOH \rightarrow CH_3O + OH$ at 25 Torr and 1 atm in temperature range of 400−1000 K in N_2 are compared with available experimental data in Figure 5a,b. The solid and dotted lines given in the figures represent the calculated results in which the heat of

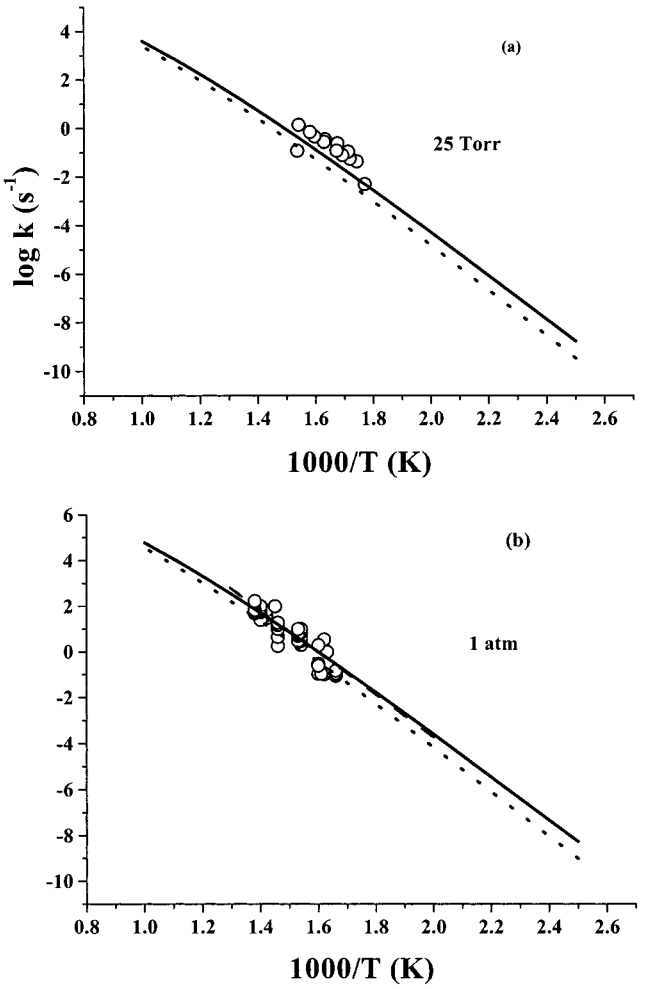

Figure 5. Predicted unimolecular rate constants for $CH_3OOH \rightarrow CH_3O + OH$ in comparison with experimental data. (a) 25 Torr N_2 pressure (data: ref 8); (b) 1 atm (data: ref 9). The solid and dotted lines in a and b represent the calculated results in which the heat of formation of CH_3O at 0 K was taken to be 5.4 and 6.8 kcal/mol, based on our recent isodemic calculations[26] and on the experimental value of Neumark and co-workers.[38] The dashed line in b represents the experimental results of Lightfoot et al.[9]

formation of CH_3O at 0 K was taken to be 5.4 and 6.8 kcal/mol, on the basis of our recent isodemic calculations[26] and on the experimental value of Neumark and co-workers,[38] respectively. Figure 5 clearly shows that our theoretically predicted rate constants at 25 Torr and 1 atm agree quite well with the available literature data[8,9] employing the heats formation of CH_3OOH and CH_3O computed by isodemic calculations. The higher heat of formation of CH_3O gives slightly small decomposition rates. The least-squares fitted theoretical expressions

$$k_c = 1.28 \times 10^{46} T^{-10.5} \exp(-25\,435/T)\ s^{-1} \qquad (25\ \text{Torr})$$

$$k_c = 1.28 \times 10^{45} T^{-9.7} \exp(-25\,970/T)\ s^{-1} \qquad (1\ \text{atm})$$

covering the temperature range of 400−1000 K. The predicted high-pressure limit rate constants for the two decomposition reactions $CH_3OOH \rightarrow CH_3O + OH$ and $CH_3OOH \rightarrow CH_2O + H_2O$ are presented in Figure 6. In the figure, our result for the former channel is seen to be in excellent agreement with the recommended value by Baulch et al.[36] The high-pressure limit rate constants for these two product channels can be expressed

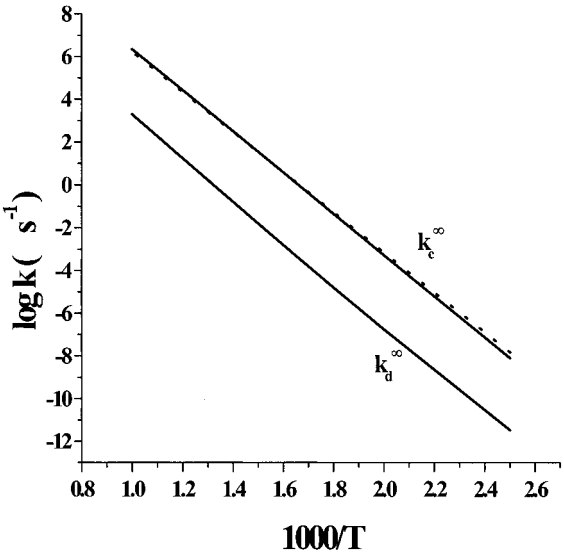

Figure 6. High-pressure limit rate constants for $CH_3OOH \rightarrow CH_3O + OH$ and $CH_2O + H_2O$. The dotted line is the recommended data of ref 36.

TABLE 4: Theoretically Predicted Total Rate Constants for CH_3OOH Decomposition at 100 Torr; 1, 10, and 50 atm, and the High Pressure Limit in N_2 in Units of s^{-1}

T (K)	100 Torr	1 atm	10 atm	50 atm	high pressure
400	3.12×10^{-9}	5.51×10^{-9}	7.14×10^{-9}	7.51×10^{-9}	7.63×10^{-9}
500	1.12×10^{-4}	2.56×10^{-4}	4.23×10^{-4}	4.86×10^{-4}	5.17×10^{-4}
550	4.52×10^{-3}	1.16×10^{-2}	2.17×10^{-2}	2.65×10^{-2}	2.95×10^{-2}
600	9.19×10^{-2}	2.61×10^{-1}	5.53×10^{-1}	7.25×10^{-1}	8.58×10^{-1}
650	1.10	3.43	8.18	1.15×10^{1}	1.48×10^{1}
700	8.74	2.94×10^{1}	7.86×10^{1}	1.20×10^{2}	1.70×10^{2}
750	4.98×10^{1}	1.80×10^{2}	5.34×10^{2}	8.77×10^{2}	1.40×10^{3}
800	2.18×10^{2}	8.41×10^{2}	2.74×10^{3}	4.84×10^{3}	8.88×10^{3}
850	7.65×10^{2}	3.13×10^{3}	1.11×10^{4}	2.11×10^{4}	4.50×10^{4}
900	2.25×10^{3}	9.66×10^{3}	3.72×10^{4}	7.52×10^{4}	1.90×10^{5}
1000	1.27×10^{4}	5.93×10^{4}	2.61×10^{5}	5.97×10^{5}	2.19×10^{6}

by

$$k_c^\infty = 2.22 \times 10^{17} T^{-0.42} \exp(-22\,457/T)\ s^{-1}$$

$$k_d^\infty = 3.09 \times 10^{-2} T^{4.51} \exp(-20\,009/T)\ s^{-1}$$

covering the temperature range 400−1000 K. Table 4 summarizes the theoretically predicted decomposition rate constants of CH_3OOH at different N_2 pressures in the temperature range of 400−1000 K.

4. Conclusion

The reaction of CH_3 with HO_2 has been studied in detail by ab initio MO and statistical theory calculations. The reaction can occur by several paths through the direct abstraction of H from HO_2 by CH_3 and the indirect association/decomposition process via CH_3OOH, producing $CH_3O + OH$ and $CH_2O + H_2O$. The direct abstraction reaction producing CH_4 and O_2 may occur via a triplet or singlet PES giving rise to the molecular oxygen in its ground electronic $^3\Sigma_g^-$ or excited $^1\Delta$ state, respectively. The reaction over the triplet surface proceeds via a van der Waals complex with a 1.9 kcal/mol binding energy and a small (1.2 kcal/mol) barrier leading to the $CH_4 + O_2$ products. We have examined the effect of multiple reflections above the complex on the predicted rate constant; it was found to be quite significant at low temperatures ($T < 300$ K). The formation of O_2 ($^1\Delta$) has a 4.1 kcal/mol reaction barrier. The

rate constants for both processes have been calculated for combustion applications in the 300−3000 K temperature range.

The formation of CH_3OOH by the CH_3-O_2H association and the decomposition of the peroxide molecule producing $CH_3O + OH$ both occur barrierlessly. Their transition states were characterized by the flexible transition-state approach with the Variflex code of Klippenstein and co-workers.[18] The production of CH_3O from $CH_3 + HO_2$ dominates the reaction, and its rate constant was found to be at least 2 orders of magnitude greater than that for CH_2O formation despite the much larger exothermicity of the latter process. These two reactions were found to be pressure-independent up to 50 atm of N_2.

The rate constants for the thermal unimolecular decomposition of CH_3OOH have been calculated and compared with the available literature data obtained at 25 Torr and atmopsheric pressure. The agreement was excellent if the heats of formation predicted by the isodesmic method for CH_3O and CH_3OOH, 5.4 ± 0.5 and -29.0 ± 1.0 kcal/mol, respectively, were employed in the calculation.

Acknowledgment. This work is sponsored partially by the Basic Energy Science, Department of Energy under Grant No. DE-FG02-97-ER14784 (to R.Z.) and partially by ONR under Grant No. N00014-89-J-1949 (to M.C.L.).

References and Notes

(1) Lloyd, A. C. *Int. J. Chem. Kinet.* **1974**, *6*, 169.
(2) Reid, I. A. B.; Robinson, C.; Smith, D. B. *Symp. (Int.) Combust., [Proc.]* **1985**, *20th*, 1833−43.
(3) Rotzoll, G. *Ger. Combust. Sci. Technol.* **1986**, *47*, 275.
(4) Hunter, T. B.; Wang, H.; Litzinger, T. A.; Frenklach, M. *Combust. Flame* **1994**, *97*, 201.
(5) Petersen, E. L.; Roehrig,; Davidson, D. F.; Hanson, R. K.; Bowman, C. T. *Symp. (Int.) Combust., [Proc.]* **1996**, *26th*, 799.
(6) Petersen, E. L.; Davidson, D. F.; Hanson, R. K. *Combust. Flame* **1999**, *117*, 272.
(7) Hwang, S. M.; Ryu, V.; Witt, K. J. De.; Rabinowitz, M. J. *J. Phys. Chem. A* **1999**, *103*, 5949.
(8) Kirk, A. D. *Can. J. Chem.* **1965**, *43*, 2236.
(9) Lightfoot, P. D.; Roussel, P.; Caralp, F.; Lesclaux, R. *J. Chem. Soc., Faraday Tran.* **1991**, *87*, 3213.
(10) Mebel, A. M.; Morokuma, K.; Lin, M. C. *J. Chem. Phys.* **1995**, *103*, 7414.
(11) Baer, T.; Hase, W. L. *Unimolecular Reaction Dynamics: Theory and Experiments*; Oxford University Press: New York, 1996.
(12) Becke, A. D. *J. Chem. Phys.* **1993**, *98*, 5648.
(13) Becke, A. D. *J. Chem. Phys.* **1992**, *96*, 2155.
(14) Becke, A. D. *J. Chem. Phys.* **1992**, *97*, 9173.
(15) Lee, C.; Yang, W.; Parr, R. G. *Phys. Rev.* **1988**, *B37*, 785.
(16) Frisch, M. J.; Trucks, G. W.; Head-Gordon, M.; Gill, P. M. W.; Wong, M. W.; Foresman, J. B.; Johnson, B. G.; Schlegel, H. B.; Robb, M. A.; Replogle, E. S.; Gomperts, T.; Andres, J. L.; Raghavachari, K.; Binkley, J. S.; Gonzales, C.; Martin, R. L.; Fox, D. J.; DeFrees, D. J.; Baker, J.; Stewart, J. J. P.; Pople, J. A. Gaussian 92/DFT, Revision B, Gaussian, Inc., Pittsburgh, PA, 1992.
(17) Werner, H.-J.; Knowles, P. J. *MOLPRO-96*; University of Sussex, Falmer: Brighton, U.K., 1996.
(18) Klippenstein, S. J.; Wagner, A. F.; Dunbar, R. C.; Wardlaw, D. M.; Robertson, S. H. *VARIFLEX*, version 1.00; 1999.
(19) Klippenstein, S. J.; Yand, D. L.; Yu, T.; Kristyan, S.; Lin, M. C. *J. Phys. Chem. A.* **1998**, *102*, 6973.
(20) Miller, J. A.; Klippenstein, S. J.; Robertson, S. H. *J. Phys. Chem. A* **2000**, *104*, 7525.
(21) Gilbert, R. G.; Smith, S. C. *Theory of Unimolecular and Recombination Reactions*; Blackwell Scientific: Carlton, Australia, 1990.
(22) Holbrook, K. A.; Pilling, M. J.; Robertson, S. H. *Unimolecular Reactions*; Wiley: New York, 1996.
(23) Troe, J. *J. Chem. Phys.* **1977**, *66*, 6745.
(24) Zhu, R. S.; Lin, M. C. *J. Phys. Chem. A* **2000,** *104* (46), 10807.
(25) Xia, W. S.; Lin, M. C. *PhysChemComm* **2000**, 13.
(26) Zhu, R. S.; Lin, M. C. *J. Chem. Phys.* **2001**, in press.
(27) Zhu, R. S.; Lin, M. C. *J. Phys. Chem. A* **2001**, submitted for publication.
(28) Varshni, V. P. *Rev. Mod. Phys.* **1957**, *29*, 664.
(29) Mourits, F. M.; Rummens, F. H. A. *Can. J. Chem.* **1977**, *55*, 3007.
(30) Hirschfelder, J. O.; Wigner, J. *Chem. Phys.* **1939**, *7*, 616.
(31) Miller, W. H. *J. Chem. Phys.* **1976**, *65*, 2216.
(32) Tsang, W.; Hampson, R. F. *J. Phys. Chem. Data* **1986**, *15*, 1087.
(33) Wardlaw, D. M.; Marcus, R. A. *Chem. Phys. Lett.* **1984**, *110*, 230; *J. Chem. Phys.* **1985**, *83*, 3462.
(34) Klippenstein, S. J.; Marcus, R. A. *J. Chem. Phys.* **1987**, *87*, 3410.
(35) Benson, S. W. *Thermochemical Kinetics*, 2nd ed.; John Wiley: Chichester, U.K., 1976.
(36) Baulch, D. L.; Cobos, C. J.; Cox, R. A.; Esser, C.; Frank, P.; Just, Th.; Kerr, J. A.; Pilling, M. J.; Troe, J.; Walker, R. W.; Warnatz, J. *J. Phys. Chem. Ref. Data* **1992**, *21*, 411.
(37) Baulch, D. L.; Cobos, C. J.; Frank, R. A. P.; Hayman, G.; Just, Th.; Kerr, J. A.; Murrells, T.; Pilling, M. J.; Troe, J.; Walker, R. W.; Warnatz, J. *J. Phys. Chem. Ref. Data* **1994**, *23*, 847.
(38) Osborn, D. L.; Leahy, D. J.; Ross, E. M.; Neumark, D. M. *Chem. Phys. Lett.* **1995**, *235*, 484.
(39) Chase, M. W., Jr. *NIST-JANAF Thermochemical Tables*, 4th ed.; Woodbury: New York, 1998.